12^{th} International Conference on Fracture Mechanics of Concrete and Concrete Structures
FraMCoS-12
B.L.A. Pichler, Ch. Hellmich, P. Preinstorfer (Eds)

https://doi.org/10.21012/FC12.1153
MS09-2:1

FROM CURING TO FIRE ACCIDENT: A NOVEL, COMPREHENSIVE MODEL FOR CONCRETE'S FIRE RESISTANCE

Stefano Dal Pont*, Giuseppe Sciumé† and Murilo H. Moreira‡

*Université Grenoble Alpes, CNRS, Grenoble INP, 3SR,
Rue de la Piscine, Grenoble, 38000, France
e-mail: stefano.dalpont@univ-grenoble-alpes.fr

†Université de Bordeaux, CNRS, Bordeaux INP, INRAE, I2M Bordeaux
Avenue d'Aquitaine, Pessac, 33607, France
e-mail: giuseppe.sciume@u-bordeaux.fr

‡Federal University of Sao Carlos, Graduate Program in Materials Science and Engineering (PPGCEM)
Rod. Washington Luiz, km 235, 13565-905, São Carlos, SP, Brazil
e-mail: murilo.moreira@estudante.ufscar.br

Key words: Thermohydrochemical Model, Early Age Concrete, Stoechiometric-based Model, Concrete Drying, Fire Resistance

Abstract. The durability of concrete under extreme temperatures is primarily influenced by the behavior of calcium silicate hydrates (C-S-H), the primary binding phase in the material. During heating, the release of chemically bound water within C-S-H leads to degradation of material properties, ultimately contributing to spalling. To accurately predict concrete's performance in fire scenarios, comprehensive thermo-hydro-chemical (THC) models are indispensable. This research presents a novel THC model that simulates the entire lifecycle of concrete, from its initial casting to potential fire accidents. The model comprehensively accounts for the interplay between temperature, humidity, and the chemical reactions taking place within the concrete microstructure. By incorporating the effects of C-S-H hydration and dehydration, the model provides a more accurate representation of concrete's behavior under various conditions. A key innovation in this work is the development of a novel adsorption-desorption model that captures the irreversible nature of chemical damage within the porous structure. This model simplifies the calibration process, requiring fewer experimental inputs. The model is validated against experimental data, demonstrating its ability to accurately predict concrete's response in both early-age behavior and high-temperature conditions. The results underscore the significant impact of the initial hygral state on the concrete's fire resistance, highlighting the importance of considering this factor in structural design and analysis, especially in real-world conditions, where the heterogeneity is high both in the water distribution and, consequentially, in the resulting microstructure. Finally, another novelty of the current work is the availability of the developed thermo-hydro-chemical code made publicly available on GitHub, facilitating its application and further research in the field of concrete fire safety.

1 INTRODUCTION

Concrete is a unique material that suits several infrastructure needs, such as nuclear containment structures, bridges, or tunnels [1]. One critical aspect of such applications is how the properties of concrete evolve over time [1–6].

A special case is its behavior under expected or accidental heating, where critical transformations can occur, involving multiscale and coupled thermal, hygral, chemical, and mechanical phenomena [7–9]. Under such conditions, the unreacted water evaporates, and the resulting hydrates from the curing process are decomposed, changing the pore structure and resulting in water vapor that can be pressurized inside the partially saturated pores. Such pore stresses are combined with thermomechanical stresses, which are believed to be related to the observed explosive spalling [8, 10]. There is no consensus about the mechanisms that drive this process and new discoveries are still under development, such as the role of flash vaporization identified by Felicetti et al. [11].

A common strategy to study this subject consists of the PTM tests, which are based on pointwise measurements of Temperature, gas Pressure and Mass lossthrough the use of transducers [12–14]. The results collected from such experiments are limited to small regions close to the sensors. Additionally, a wide range of values is measured, around 0.3-3.5 MPa for similar concrete compositions [15, 16], which poses concerns over the reproducibility of such measurements in representing what really happens in heated bodies with no sensors.

As an alternative, full-field techniques such as X-ray and neutron tomography were proposed and led to important advances such as proving the existence of the moisture clogging phenomenon (an accumulation of water at colder regions of the body in which condensation can locally reduce the material permeability) and highlighting the impact of localized heterogeneities, such as aggregates, on moisture transport [17–19].

The sample size limitations for studies in controlled environments have highlighted the appeal of numerical models capable of predicting the behavior of concrete during heating. These were developed in recent years [9, 20–22], and currently consist of multiphase-coupled models which despite drawbacks such as a semi-empirical nature (e.g. requiring parameters to be calibrated) and the use of many phenomenological laws, were proved quite effective in reproducing experimental results [9, 21, 23–25].

Nonetheless, in such endeavors, one critical simplifying assumption is the consideration of uniform initial conditions that represent a virgin-state material. This is problematic for two reasons: first, from the casting stage throughout its service life, concrete is exposed to varying environmental conditions that can influence moisture distribution, and result in differential curing, micro-cracks coalescence or creep [26] and second, the concrete ages with time and structures with distinct history can have different resulting microstructures [27].

Such aspects, which are especially critical during the young age stage of concrete, were already studied using numerical models aimed at predicting the evolving chemical and physical characteristics of concrete at room temperatures [28–31]. Such models, however, were limited to analysis at mild temperatures (40 °C at most), and were not capable of predicting dehydration.

More than a simple combination of the already existing young age and high temperature models is required to accurately predict the complex behavior of concrete. What is needed is a unified numerical framework that can model the cement hydration and its eventual decomposition at higher temperatures and is capable of analyzing the impact of the mid and long-term behavior in the explosive spalling. Thus, the current work implements a thermohygrochemical model based on the stoichiometric approach by Powers et al. [32], in which the constitutive equations that describe the concrete porosity, its hydration degree, and the moisture content are directly derived from its composition.

Simple experiments such as calorimetry and thermogravimetry can be used to calibrate such relations, highlighting a more straightforward alternative to the manual calibration of the concrete properties to fit PTM data. An additional contribution of this study is a new way to implement the temperature effect and the chemical

damage irreversibility of the porous microstructure in the sorption/desorption isotherms. This novel strategy also addresses the strong discontinuities found around the critical temperature of water, yielding a more numerically robust formulation.

2 NUMERICAL MODEL

2.1 Overview

The detailed development of the model can be found in [33]. The current section briefly introduces the main unique features of the proposed formulation. Following the same theoretical basis from other thermohygro models for concrete at high temperatures, the model is built upon the hybrid mixture theory for porous media, using a continuously homogenized framework [33].

The balance equations considered follow the formulation presented in [34, 35], which was then extended by Sciumé [36]. Numerically, the model consists of a fully coupled monolithic system of four partial derivative equations which are solved using the FEniCS finite element software [37]. The primary variables are the gas and capillary pressures, p_g and p_c, the temperature and the hydration degree, G. The code is available in a GitHub repository at: `https://github.com/ANR-MultiFIRE/THC/`.

2.2 Cement paste hydration and aging: extension to high temperatures

Following the chemical model that depicts the cement hydration and the aging as proposed by Sciumè et al. [36], the hydration degree of the sample Γ is given by:

$$\Gamma(t) = \frac{m_{hyd}(t)}{m^{\infty}_{hyd}} \tag{1}$$

where $m_{hyd}(t)$ is the chemically bound water at time t and m^{∞}_{hyd} is such quantity at $t \to \infty$.

As the microstructure evolution in concrete is dependent on the hydrates formed during curing, the degree of hydration, Γ describes the full hydration (and dehydration) process of the cement paste. Thus, this is the main internal variable of the thermohygrochemical (THC) model.

The chemical hydration reaction of cement can be described following the Arrhenius law:

$$\frac{d\Gamma}{dt} = A_{\Gamma}(\Gamma)\beta_{RH}(RH)\exp\left(-\frac{E_a}{RT}\right) \tag{2}$$

where $A_{(\Gamma)}$ represents the macroscopic chemical affinity (as defined in [36]), E_a denotes the activation energy for hydration, and β is a parameter dependent on the relative humidity RH, accounting for its influence on the reaction. As the chemical affinity is also a function of the hydration degree, in the current implementation, an equation is solved for the evolution of Γ, where G is an internal variable that represents the hydration degree, as described by Gawin et al. [22].

The dehydration hydration are consistently defined by introducing a dehydration degree F, that, combined with Γ defines the effective hydration degree $\tilde{\Gamma}$:

$$\tilde{\Gamma} = (1 - F(T))\Gamma \tag{3}$$

The coupled evolution model is therefore expressed by the following relationship, with a conditional behavior introduced to enforce irreversibility of the dehydration [33]:

$$\frac{d\tilde{\Gamma}}{dt} = (1 - F)\frac{d\Gamma}{dt} - \Gamma\frac{dF}{dt} \tag{4}$$

Different laws that represent $F(T)$ can be found in the literature. The current work assumes the one proposed by Pesavento et al. [21], with the parameters calibrated to reproduce the results by Kalifa et al. [12]. The used parameters are fully described in [33].

In order to quantify the volumetric fractions of the different phases, Powers' model is considered. The initial volume fraction of water in the mixture is given by:

$$p = \frac{w/c}{w/c + \rho_w/\rho_c + (\rho_w/\rho_{sf})(s/c)} \tag{5}$$

with w, c, sf being the mass fraction of water, cement and silica fume, and ρ_i the density of

phase i. The k parameter considered in Power's model is defined as:

$$k = \frac{1}{1 + \rho_c/\rho_{sf}(s/c)} \tag{6}$$

2.3 Porosity evolution

By assuming a full cement hydration, ξ_∞, the total porosity of the cement paste as a function of the hydration degree is given by:

$$\phi(\tilde{\Gamma}) = \phi_\infty^{cp}\,\Omega + a_\phi(1-\tilde{\Gamma})\,\Omega + \phi^{As}\,(1-\Omega) \tag{7}$$

where Ω is the volume of the cement paste, ϕ^{As} is the average porosity of the aggregates (usually neglected) and ϕ_∞^{cp} is the final value of the cement paste porosity after curing. ϕ_∞^{cp} and a_ϕ are given by:

$$\phi_\infty^{cp} = p - k[0.52 - 0.69(s/c)](1-p)\,\xi_\infty \tag{8}$$

$$a_\phi = k[0.52 - 0.69(s/c)](1-p)\,\xi_\infty \tag{9}$$

2.4 Sorption/desorption isotherms

To describe the amount of free water in the concrete, S_l, the sorption/desorption isotherms are considered. Considering a relationship similar to the one proposed by Baroghel-Bouny [38], it can be found as a function of the temperature, the capillary pressure, p_c, and the saturation degree as follows:

$$S_l(p_c, T, \tilde{\Gamma}) = \left[\left(\frac{p_c}{a(T,\tilde{\Gamma})}\right)^{\frac{b}{b-1}} + 1\right]^{-\frac{1}{b}} \tag{10}$$

The coefficients a and b are fitting parameters related to the material type. The traditional function to represent the dependence of the a term with temperature has a strong discontinuity at the critical temperature of water as shown in Figure 1.

The relationship devised herein is based on recent findings and is given by:

$$a(T,\tilde{\Gamma}) = a_0\left(\frac{\tilde{\Gamma} + a_1^a}{1 + a_1^a}\right)^{a_2^a} \frac{\gamma^w(T) + a_3^a\,\gamma_0^w}{(1 + a_3^a)\,\gamma_0^w} \tag{11}$$

where $a_1^a = 0.1$ and $a_2^a = 1.5$ for the composition in Kalifa's test, and the last term was disregarded.

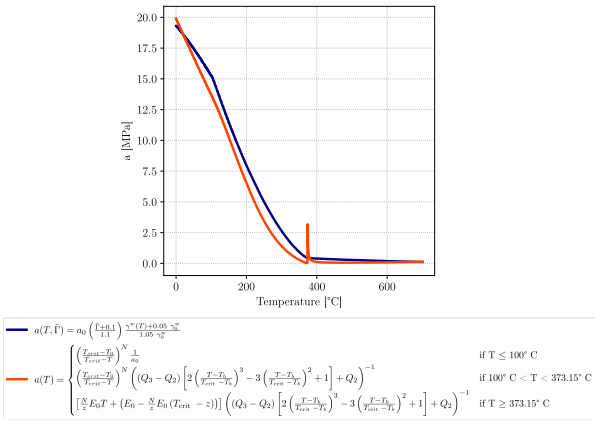

Figure 1: Comparison of the currently proposed saturation degree coefficient law and the one adopted by Gawin et al. [22].

2.5 Final form of the conservation equations

The final form of the mathematical problem defined through three conservation equations (mass balance of dry air, of water and enthalpy balance) and also the evolution equation of the dehydration degree. The development is presented in [33] and it comprises Darcy's, Fick's and Fourier's laws to account for the mass and heat transfer fluxed. The final form is shown below:

• Dry air:

$$\begin{aligned}\phi(1-S_l)\left(\frac{\partial\rho_a}{\partial T}\frac{\partial T}{\partial t}+\frac{\partial\rho_a}{\partial p_c}\frac{\partial p_c}{\partial t}+\frac{\partial\rho_a}{\partial p_g}\frac{\partial p_g}{\partial t}\right)-\\ -\phi\rho_a\left(\frac{\partial S_l}{\partial T}\frac{\partial T}{\partial t}+\frac{\partial S_l}{\partial p_c}\frac{\partial p_c}{\partial t}+\frac{\partial S_l}{\partial\tilde{\Gamma}}\frac{\partial\tilde{\Gamma}}{\partial t}\right)-\nabla\cdot\left(K\frac{\rho_a k_{rg}}{\mu_g}\nabla p_g\right)-\\ -\nabla\cdot\left(D\rho_g\frac{M_v M_a}{M_g^2}\nabla\left(\frac{p_a}{p_g}\right)\right)=(1-S_l)\rho_a\left(a_\phi\Omega\frac{\partial\tilde{\Gamma}}{\partial t}\right)\end{aligned} \tag{12}$$

• Total water:

$$\begin{aligned}\phi(\rho_l-\rho_v)\left(\frac{\partial S_l}{\partial T}\frac{\partial T}{\partial t}+\frac{\partial S_l}{\partial p_c}\frac{\partial p_c}{\partial t}+\frac{\partial S_l}{\partial\tilde{\Gamma}}\frac{\partial\tilde{\Gamma}}{\partial t}\right)+\\ +(1-S_l)\phi\left(\frac{\partial\rho_v}{\partial T}\frac{\partial T}{\partial t}+\frac{\partial\rho_v}{\partial p_c}\frac{\partial p_c}{\partial t}+\frac{\partial\rho_v}{\partial p_g}\frac{\partial p_g}{\partial t}\right)+S_l\phi\frac{\partial\rho_l}{\partial T}\frac{\partial T}{\partial t}-\\ -\nabla\cdot\left(K\frac{\rho_l k_{rl}}{\mu_l}\left(\nabla p_g-\nabla p_c\right)\right)-\nabla\cdot\left(K\frac{\rho_v k_{rg}}{\mu_g}\nabla p_g\right)-\nabla\cdot\left(D\rho_g\frac{M_v M_a}{M_g^2}\nabla\left(\frac{p_v}{p_g}\right)\right)=\\ =\left[S_l\rho_l+(1-S_l)\rho_v\right]\left(a_\phi\Omega\frac{\partial\tilde{\Gamma}}{\partial t}\right)-0.228c\xi_\infty\frac{\partial\tilde{\Gamma}}{\partial t}\end{aligned} \tag{13}$$

• Energy conservation:

$$\begin{aligned}\overline{\rho C_p}\frac{\partial T}{\partial t}+K\left(C_{p,l}\frac{\rho_l k_{rl}}{\mu_l}\left(\nabla p_g-\nabla p_c\right)+C_{p,g}\frac{\rho_v k_{rg}}{\mu_g}\nabla p_g\right)\cdot\nabla T-\\ -\nabla\cdot(\lambda\cdot\nabla T)-H_{vap}S_l\phi\frac{\partial\rho_l}{\partial T}\frac{\partial T}{\partial t}-\\ -H_{vap}\rho_l\phi\left(\frac{\partial S_l}{\partial T}\frac{\partial T}{\partial t}+\frac{\partial S_l}{\partial p_c}\frac{\partial p_c}{\partial t}+\frac{\partial S_l}{\partial\tilde{\Gamma}}\frac{\partial\tilde{\Gamma}}{\partial t}\right)-H_{vap}\nabla\cdot\left(K\frac{\rho_l k_{rl}}{\mu_l}\left(\nabla p_g-\nabla p_c\right)\right)=\\ =\quad -H_{vap}S_l\rho_l\left(a_\phi\Omega\frac{\partial\tilde{\Gamma}}{\partial t}\right)+\left(H_{vap}0.228c\xi_\infty+L_{hyd}\right)\frac{d\tilde{\Gamma}}{dt}\end{aligned} \tag{14}$$

Lastly, the evolution equation for the hydration degree is defined, where G represents an internal variable used to explicitly determine $\Gamma(t)$. This formulation leads to a mathematical problem described by the system of Equations (12 - 15). • Evolution of the hydration degree:

$$\frac{\partial\Gamma}{\partial t}=\frac{\partial G}{\partial t} \tag{15}$$

2.6 Boundary conditions

To solve the mathematical problem over the domain Ω, the following set of boundary conditions are considered on $\Sigma=\partial\Omega$ [39]:

$$p_g=\bar{p}_g \ \text{ on } \ \Sigma_p \tag{16}$$

$$p_c=\bar{p}_c \ \text{ on } \ \Sigma_p \tag{17}$$

$$T=\bar{T} \ \text{ on } \ \Sigma_T \tag{18}$$

$$-\boldsymbol{J}_{v-s}\cdot\boldsymbol{n}=\bar{q}_v-h_g\left(\rho_v-\rho_v^\infty\right) \ \text{ on } \ \bar{\Sigma}_p \tag{19}$$

$$-\boldsymbol{J}_{a-s}\cdot\boldsymbol{n}=\bar{q}_a-h_g\left(\rho_a-\rho_a^\infty\right) \ \text{ on } \ \bar{\Sigma}_p \tag{20}$$

$$-\boldsymbol{J}_{l-s}\cdot\boldsymbol{n}=\bar{q}_l \ \text{ on } \ \bar{\Sigma}_p \tag{21}$$

$$\begin{aligned}-\left(\boldsymbol{q}-H_{vap}\boldsymbol{J}_{l-s}\right)\cdot\boldsymbol{n}=\bar{q}_T-\\ -h_T\left(T-T_\infty\right)-\\ -\epsilon\sigma\left(T^4-T_\infty^4\right) \ \text{ on } \ \bar{\Sigma}_T\end{aligned} \tag{22}$$

where $\Sigma_\bullet$ is part of the boundary where Dirichlet boundary conditions are considered whereas $\bar{\Sigma}_\bullet$ is its complementary part (with unit outward normal $\boldsymbol{n}$) where the mass and heat fluxes are prescribed.

The vapor and air fluxes are represented by $\bar{q}_\pi$ with $\pi = v, a$, ρ_π^∞ is the densities of vapor and dry air, the temperature in the far field surrounding gas is given by T_∞, while h_g and h_T are the convective mass/energy exchange coefficient, respectively [39]. ϵ is the emissivity and σ is the Stefan-Boltzmann constant.

The set of initial conditions for the transient problem is defined too, with $\boldsymbol{x}$ representing the vector of spatial coordinates: $p_g(\boldsymbol{x}, t=0)$, $p_c(\boldsymbol{x}, t=0)$, $T(\boldsymbol{x}, t=0)$, and $G(\boldsymbol{x}, t=0)$.

The right-hand side of Equation (22) represents the interface exchange between the porous medium and the surrounding fluid (e.g., moist air), whereas the second term on the left-hand side accounts for the energy exchange associated with vaporization.

Finally, it should be considered that relationships between the densities of the distinct phases and the state variables are non-linear, and consequentially, the numerical implementation of such boundary conditions requires a linearization of such quantities as described in [33, 34]. The finite element formulation is detailed in [33]

3 NUMERICAL ANALYSIS

The current work numerical analysis considers an experimental benchmark focused on the mass loss of a concrete specimen, alongside the simulation of various scenarios to evaluate their impact on the results. This specific test, standardized for laboratory-scale experiments, was chosen due to its relevance and reliability [40, 41]. It uses cylindrical specimens with dimensions of 16 cm in diameter and 32 cm in height, tested after 28 days of curing. Simulations were performed for multiple aging durations to assess whether conducting the test at different curing times would yield significant variations. Figure 2 illustrates the geometry analyzed, details the boundary conditions at each stage, and provides an overview of the scenarios considered. A complete list of the material properties considered for the current simulations is given in [33].

A 2D axisymmetric unstructured triangular mesh consisting of 688 linear continuous Galerkin elements was used to model the sample, as depicted in Figure 2 (a). The simulation followed the experimental methodology outlined in [42], comprising four distinct stages: initial curing with impermeable boundaries, aging in a high-humidity environment (with the sample immersed in water in this case), heating, and cooling. The boundary conditions for each stage are specified in Figure 2 (b). Four scenarios were analyzed, varying the aging durations to 7, 14, 28, and 180 days, as shown in Figure 2 (c). Experimental results from Scenario 3, which represents the one reported by Kanema et al., are compared with simulation results in Figure 3.

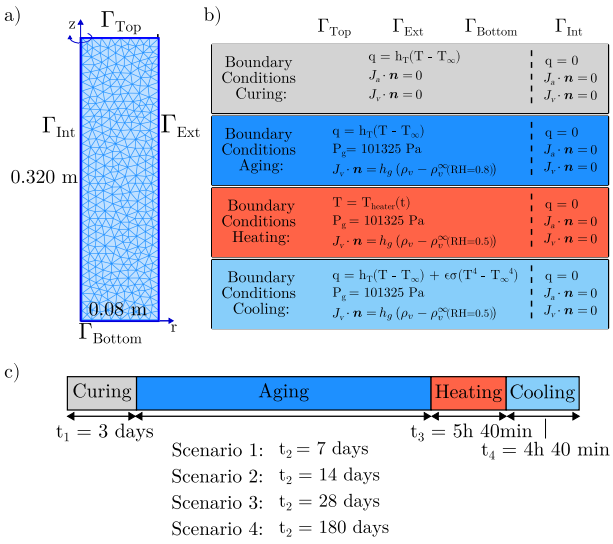

Figure 2: a) Domain of the axisymmetric simulation, b) set of the boundary conditions and corresponding stages and c) representation of the different scenarios analyzed.

Apart from the cooling, the use of the Dirichlet boundary condition, Equation 18, during the heating stage guarantees that the experimental surface temperatures are reproduced by the model, as shown in Figure 3 (a). The thermal evolution predicted at the center of the sample

agrees well with the measure values until the 5h mark, when the simulation begins to overestimate the temperature increase. These discrepancies are further highlighted in Figure 3 (b), which tracks the temperature difference between the surface and the center of the sample.

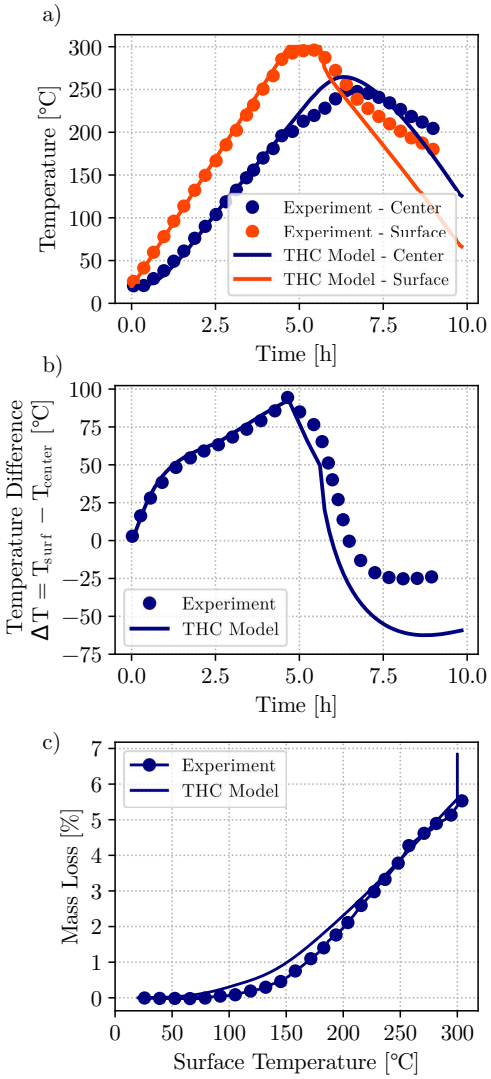

Figure 3: a) Temperature evolution at the sample's center and surface, b) evolution of temperature difference between surface and center and c) mass loss as a function of the sample temperature.

Figure 3 (c), shows the mass loss dynamics, indicating that the THC model effectively captures the overall water removal process, with faster drying observed between 75 °C and 225 °C. Refinements to the constitutive equations describing the material composition could align the simulation and experimental results more closely. However, a notable discrepancy exists during the one-hour plateau at 300 °C, where the model predicts a mass loss of nearly 1%, contrasting with the negligible mass loss observed experimentally.

Despite these differences, the model successfully reproduces the experimentally measured mass loss using only the initial formulation of the concrete composition and the applied boundary conditions. This capability underscores the potential of the current THC model for replacing traditional experiments with numerical simulations.

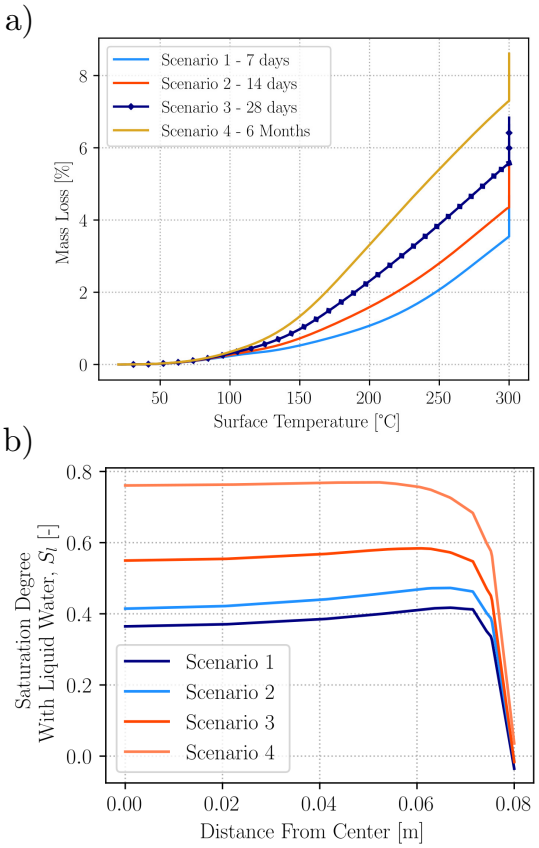

Figure 4: a) Mass loss of samples after 7 days, 14 days, 28 days and 6 months. b) Saturation degree with liquid water distribution at the center line of the sample when the surface temperature is 120° C.

The influence of different aging durations is examined in Figure 4 (a), which shows the mass loss for the four scenarios. In the temperature interval between 20° C and 120 °C, the mass loss curves are nearly identical across all

scenarios. This behavior can be attributed to the fact that, at these temperatures, the drying front has not yet penetrated the sample's interior, where the differences in saturation degree are most pronounced. This effect is further detailed in Figure 4 (b).

After that, a clear trend between the increase in the aging duration and larger mass losses was observed as the longer the sample was kept in contact with water, the larger the sample water intake.

4 CONCLUSIONS

The behavior of concrete is not static: the long and incomplete hydration reactions that start after mixing continue throughout its service life, and it is impacted by the surrounding environmental conditions. Consequently, its hygral state and the microstructure are also transient and reflect this transient nature.

The current work investigated the influence of age and history on concrete high-temperature behavior, with a novel fully coupled thermo-hygro-chemical model. The developed framework, based on properties widely available in the literature, accounts for the effects of temperature and relative humidity on the chemical evolution of concrete properties. Its numerical implementation was validated by simulating an experimental mass loss test.

In addition, a novel retention curve law was proposed to eliminate discontinuities found in previous implementations. This improved constitutive law enhances numerical stability, which is particularly critical for strongly nonlinear problems under extreme conditions such as fire or nuclear reactor accidents. By incorporating the hydration development during concrete aging, the model enables the evaluation of multiple scenarios with varying aging durations. For samples aged in high relative humidity environments, mass loss was found to vary by up to 4.5 wt.

The proposed THC model has significant potential to uncover key relationships specially when considering the intrinsic hetergeneity of concrete and how that impacts its high-temperature behavior. This will also be especially relevant for massive concrete structures, which may require years to achieve hygral equilibrium. Future studies will extend the analysis to real accident scenarios at the structural scale, accounting for these effects.

Ultimately, this work offers a robust alternative to the contentious yet widely used approach of relying on incoherent material datasets from the literature and calibrating constitutive laws using PTM tests, which may lack reliability. The methodology presented here employs a limited number of straightforward characterization tests, producing a consistent material dataset and simplifying the calibration process. By adopting this approach, most standard high-temperature experiments could be replaced by numerical simulations, allowing resources to be redirected toward innovative testing rather than routine characterization.

5 SUPPLEMENTARY CODE

Supplementary Code The supplementary code for the workflows can be found in the following GitHub repository:

`https://github.com/ANRMultiFIRE/THC`

6 ACKNOWLEDGMENTS

This study was financed in part by the Coordenação de Aperfeiçoamento de Pessoal de Nível Superior - Brasil (CAPES) - Finance Code 001 and the Agence National pour la Recherche (ANR) - project ANR-23-CE51-0001. The authors would like to thank the Fundação de Amparo à Pesquisa do Estado de São Paulo - FAPESP (grant numbers: 2021/00251-0 and 2022/12406-0).

REFERENCES

[1] D L Fillmore. Literature review of the effects of radiation and temperature on the aging of concrete. Technical report, Idaho National Lab.(INL), Idaho Falls, ID (United States), 2004.

[2] D L Fillmore, P L Winston, S L Morton,

C R Hoffman, L A Van Ausdeln, T Saegusa, K Shirai, T Hattori, and A Sasahara. The long-term performance of concrete in nuclear applications. In *ASME Pressure Vessels and Piping Conference*, volume 41928, pages 639–648, 2005.

[3] J Moore, J Tcherner, D Naus, M Bakirov, Jari Puttonen, and I Moga. *Aging management of concrete structures in nuclear power plants*. IASMiRT, 2015.

[4] V Di Murro, L Pelecanos, K Soga, C Kechavarzi, R F Morton, and L Scibile. Long-term deformation monitoring of cern concrete-lined tunnels using distributed fibre-optic sensing. *Geotechnical Engineering Journal of the SEAGS & AGSSEA*, 50(1), 2019.

[5] W Liu, J Chen, Y Luo, L Chen, L Zhang, C He, Z Shi, Z Xu, H Zhu, and T Hu. Long-term stress monitoring and in-service durability evaluation of a large-span tunnel in squeezing rock. *Tunnelling and Underground Space Technology*, 127:104611, 2022.

[6] I Maruyama, H Sasano, Y Nishioka, and G Igarashi. Strength and young's modulus change in concrete due to long-term drying and heating up to 90 c. *Cement and Concrete Research*, 66:48–63, 2014.

[7] Z P Bažant. Instability, ductility, and size effect in strain-softening concrete. *Journal of the engineering mechanics division*, 102(2):331–344, 1976.

[8] R Jansson. *Fire spalling of concrete: theoretical and experimental studies*. PhD thesis, KTH Royal Institute of Technology, 2013.

[9] S Dal Pont and A Ehrlacher. Numerical and experimental analysis of chemical dehydration, heat and mass transfers in a concrete hollow cylinder submitted to high temperatures. *International Journal of Heat and Mass Transfer*, 47(1):135 – 147, 2004.

[10] MH Moreira, S Dal Pont, R Ausas, AP Luz, T Cunha, C Parr, and VC Pandolfelli. Main trends on the simulation of the drying of refractory castables-review. *Ceramics International*, 47(20):28086–28105, 2021.

[11] Roberto Felicetti, Ramin Yarmohammadian, Stefano Dal Pont, and Alessandro Tengattini. Fast vapour migration next to a depressurizing interface: A possible driving mechanism of explosive spalling revealed by neutron imaging. *Cement and Concrete Research*, 180:107508, 2024.

[12] P Kalifa, F D Menneteau, and D Quenard. Spalling and pore pressure in HPC at high temperatures. *Cement and Concrete Research*, 30(12):1915 – 1927, 2000.

[13] S Dal Pont, H Colina, A. Dupas, and A Ehrlacher. An experimental relationship between complete liquid saturation and violent damage in concrete submitted to high temperature. *Magazine of Concrete Research*, 57(8):455–461, 2005.

[14] M R Bangi and T Horiguchi. Pore pressure development in hybrid fibre-reinforced high strength concrete at elevated temperatures. *Cement and Concrete Research*, 41(11):1150–1156, 2011.

[15] D Dauti. *A combined experimental and numerical approach to spalling of high performance concrete due to fire*. PhD thesis, Université Grenoble Alpes, 2018.

[16] D Dauti, A Tengattini, S Dal Pont, N Toropovs, M Briffaut, and B Weber. Some observations on testing conditions of high-temperature experiments on concrete: an insight from neutron tomography. *Transport in Porous Media*, 132:299–310, 2020.

[17] D Dauti, A Tengattini, S Dal Pont, N Toropovs, M Briffaut, and B Weber. Analysis of moisture migration in concrete at high temperature through in-situ neutron tomography. *Cement and Concrete Research*, 111:41 – 55, 2018.

[18] H Sleiman, A Tengattini, M Briffaut, B Huet, and S Dal Pont. Simultaneous x-ray and neutron 4d tomographic study of drying-driven hydro-mechanical behavior of cement-based materials at moderate temperatures. *Cement and Concrete Research*, 147:106503, 2021.

[19] M H Moreira, S Dal Pont, A Tengattini, A P Luz, and V C Pandolfelli. Experimental proof of moisture clog through neutron tomography in a porous medium under truly one-directional drying. *Journal of the American Ceramic Society*, 105(5):3534–3543, 2022.

[20] Z P Bažant and W Thonguthai. Pore pressure and drying fo concrete at high temperature. *Journal of Engineering Mechanics - ASCE*, 104(5):1059–1079, 10 1978.

[21] F Pesavento. *Nonlinear modelling of concrete as a multiphase material in high temperature conditions*. PhD thesis, Universita degli Studi di Padova, 2000.

[22] D Gawin, F Pesavento, and B A Schrefler. What physical phenomena can be neglected when modelling concrete at high temperature? a comparative study. part 1: Physical phenomena and mathematical model. *International Journal of Solids and Structures*, 48(13):1927 – 1944, 2011.

[23] C T Davie, C J Pearce, and N Bićanić. Coupled heat and moisture transport in concrete at elevated temperatures - effects of capillary pressure and adsorbed water. *Numerical Heat Transfer, Part A: Applications*, 49(8):733–763, 2006.

[24] K G Fey, I Riehl, R Wulf, and U Gross. Experimental and numerical investigation of the first heat-up of refractory concrete. *International Journal of Thermal Sciences*, 100:108–125, 2016.

[25] D Dauti, A Tengattini, S Dal Pont, N Toropovs, M Briffaut, and B Weber. Analysis of moisture migration in concrete at high temperature through in-situ neutron tomography. *Cement and Concrete Research*, 111:41–55, 2018.

[26] A Jkedrzejewska, F Benboudjema, L Lacarrière, M Azenha, D Schlicke, S Dal Pont, A Delaplace, J Granja, K Hajkova, and P Joachim Heinrich. Cost tu1404 benchmark on macroscopic modelling of concrete and concrete structures at early age: Proof-of-concept stage. *Construction and Building Materials*, 174:173–189, 2018.

[27] G Sciumé. *Thermo-hygro-chemo-mechanical model of concrete at early ages and its extension to tumor growth numerical analysis*. PhD thesis, Università degli studi (Padoue, Italie), 2013.

[28] Weijie You, Fengping Zhang, Yue Huang, Mi Gao, Chengqian Wen, and Guotao Yang. A coupled hygro-thermo-mechanical model for the evolution of saturation in early-age concrete. *International Journal of Heat and Mass Transfer*, 156:119817, 2020.

[29] Weijie You, Xiaoyang Liu, Huaishuai Shang, and Guotao Yang. Evolution of temperature, humidity and deformation in early-age cement-based materials based on a multi-field model. *Construction and Building Materials*, 290:123277, 2021.

[30] Minfei Liang, Ze Chang, Shan He, Yu Chen, Yidong Gan, Erik Schlangen, and Branko Šavija. Predicting early-age stress evolution in restrained concrete by thermo-chemo-mechanical model

and active ensemble learning. *Computer-Aided Civil and Infrastructure Engineering*, 37(14):1809–1833, 2022.

[31] Silvio Prskalo, Michael Helmut Gfrerer, and Martin Schanz. Multiphasic model of early stage hydration in concrete using the theory of porous media. *PAMM*, page e202300220, 2023.

[32] T C Powers and T L Brownyard. Studies of the physical properties of hardened portland cement paste. *Bulletin 22, Research Laboratories of the Portland Cement Association*, 43(9):101–132, 1946.

[33] Giuseppe Sciumè, Murilo Henrique Moreira, and Stefano Dal Pont. Thermo-hygro-chemical model of concrete: from curing to high temperature behavior. *Materials and structures*, 57(8):186, 2024.

[34] S Dal Pont, S Durand, and B A Schrefler. A multiphase thermo-hydro-mechanical model for concrete at high temperatures—finite element implementation and validation under {LOCA} load. *Nuclear Engineering and Design*, 237(22):2137 – 2150, 2007.

[35] S Dal Pont, F Meftah, and B A Schrefler. Modeling concrete under severe conditions as a multiphase material. *Nuclear Engineering and Design*, 241(3):562 – 572, 2011.

[36] G Sciumè, F Benboujema, C De Sa, F Pesavento, and Y. Birthaud. A multiphysics model for concrete at early age applied to repairs problems. *Engineering Structures*, 57:374 – 387, 2013.

[37] S Martin, J Blechta, J Hake, A Johansson, B Kehlet, A Logg, C Richardson, J Ring, M Rognes, and G N Wells. The FEniCS Project version 1.5. *Archive of Numerical Software*, 3(100), 2015.

[38] V Baroghel-Bouny, M Mainguy, T Lassabatere, and O Coussy. Characterization and identification of equilibrium and transfer moisture properties for ordinary and high-performance cementitious materials. *Cement and Concrete Research*, 29(8):1225 – 1238, 1999.

[39] R W Lewis and B A Schrefler. *The finite element method in the static and dynamic deformation and consolidation of porous media*. John Wiley & Sons, 1998.

[40] P Pliya, A L Beaucour, and A Noumowé. Contribution of cocktail of polypropylene and steel fibres in improving the behaviour of high strength concrete subjected to high temperature. *Construction and building materials*, 25(4):1926–1934, 2011.

[41] A Noumowe, M V G de Morais, M Kanema, J L Gallias, and R Cabrillac. Heat and mass transfers in a heated concrete element: 20 to 600° c. In *Fluids Engineering Division Summer Meeting*, volume 47500, pages 1007–1013, 2006.

[42] M Kanema, M V G De Morais, A Noumowe, J L Gallias, and R Cabrillac. Experimental and numerical studies of thermo-hydrous transfers in concrete exposed to high temperature. *Heat and Mass Transfer*, 44:149–164, 2007.